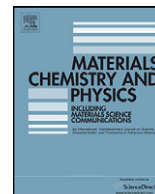




Contents lists available at ScienceDirect

Materials Chemistry and Physics

journal homepage: www.elsevier.com/locate/matchemphysReverse-loop impedance profile in Bi₂S₃ quantum dots

K.A.Z. Syed Abuthahir, R. Jagannathan*

Luminescence Group, CECRI, Karaikudi 630006, T.N., India

ARTICLE INFO

Article history:

Received 16 June 2009
Received in revised form
18 December 2009
Accepted 8 January 2010

Keywords:

Nano-structures
Optical properties
Electrochemical properties
Chalcogenides
Semiconductors

ABSTRACT

Bismuth sulfide quantum dots ($\phi \sim 12$ nm) with two-dimensional platelet morphology synthesized using a simple aqueous colloidal method exhibit directional growth along (2 1 1) direction. Impedance characteristics of this two-dimensional quantum structure yields a characteristic semi-circular profile due to a classical Voigt element in addition to a semi-circle like loop in the negative imaginary part of the impedance Nyquist plot. The apparent inductive reverse-loop impedance profile observed, a distinguishing feature of this study can be explained on the basis of an unusual negative resistor–capacitor combination, realized due to relaxation of surface states in this technologically important semiconductor–quantum structure.

© 2010 Elsevier B.V. All rights reserved.

1. Introduction

There is an ever growing research interest on bismuth sulfide Bi₂S₃ chalcogenides offering scope for numerous applications ranging from conventional thermoelectric generator [1] and photovoltaics [2] to very recent X-ray computed tomography-based imaging applications [3]. Also increased application potential of this system in other fields such as photo-sensors [4], photo-detectors [5] has propelled numerous syntheses strategies to fine-tune the desired material, physico-chemical properties through control on morphology, size and nano-architecture hierarchy of the system such as nanorods, nano-wires, nano-ribbons, nano-flowers, etc., have been tried [6–11]. Bi₂S₃ having a bulk bandgap $E_g \sim 1.3$ eV is a direct bandgap semiconductor system [12], hence size miniaturization leading to quantum structures would be of interest for opto-electronic devices. In semiconductor nanocrystals, surface states (SS) play an important role in determining several interesting properties of nano-structured materials. Hence, information on relaxation of surface states would be much useful to predict and fine-tune the material characteristics for desired application(s). The behavior of surface states showing temporal characteristics holds the key for many interesting opto-electronic properties. Notwithstanding extensive literature on the role of surface states in several nanocrystals, there seems to be no attempt using AC impedance studies to follow the relaxation of surface states in nano-structured materials. Hence, we are motivated to investigate the relaxation

behavior of surface states of this important semiconductor system having wide-range of application prospects. In this study using impedance spectroscopy, the more crucial feature is the observation of a conventional semi-circular profile in the first quadrant along with a semi-circular loop in the fourth quadrant of the complex impedance plane. This loop in the fourth quadrant is often attributed to an inductive behavior of the system and modeled by an inductive network. The prominent semi-circular feature is modeled by a Voigt element.

Furthermore, the bismuth sulfide nano-structure exhibits a strong anisotropic growth characteristics and 2D crystal habit due to its layered crystal structure. Also in view of large Bohr exciton size, this low bandgap semiconductor system exhibits a strong quantum confinement behavior and hence we thought exploring the impedance behavior for this low dimensional quantum structure would be of much fundamental importance.

2. Nano-synthesis and characterization

Bi₂S₃ nanocrystals investigated in this work were synthesized using a direct aqueous colloidal method and characterized as schematized in Fig. 1. Although it was possible to synthesize bismuth sulfide nanocrystals having wide ranging size in the 5–20 nm range, chemical compositions of the reactant aqueous solutions used in the present study were optimized to yield particles of size around ~ 12 nm. Nano-particles of larger size settled down faster, there by limiting the scope of the study and also these larger particles lie in the weak quantum confined regime. Hence, in this report we focussed our study of nano-particles of size in the range of ~ 12 nm and will be referred as nBiS in the subsequent sec-

* Corresponding author. Fax: +91 4565 227713.

E-mail address: jags57.99@yahoo.com (R. Jagannathan).

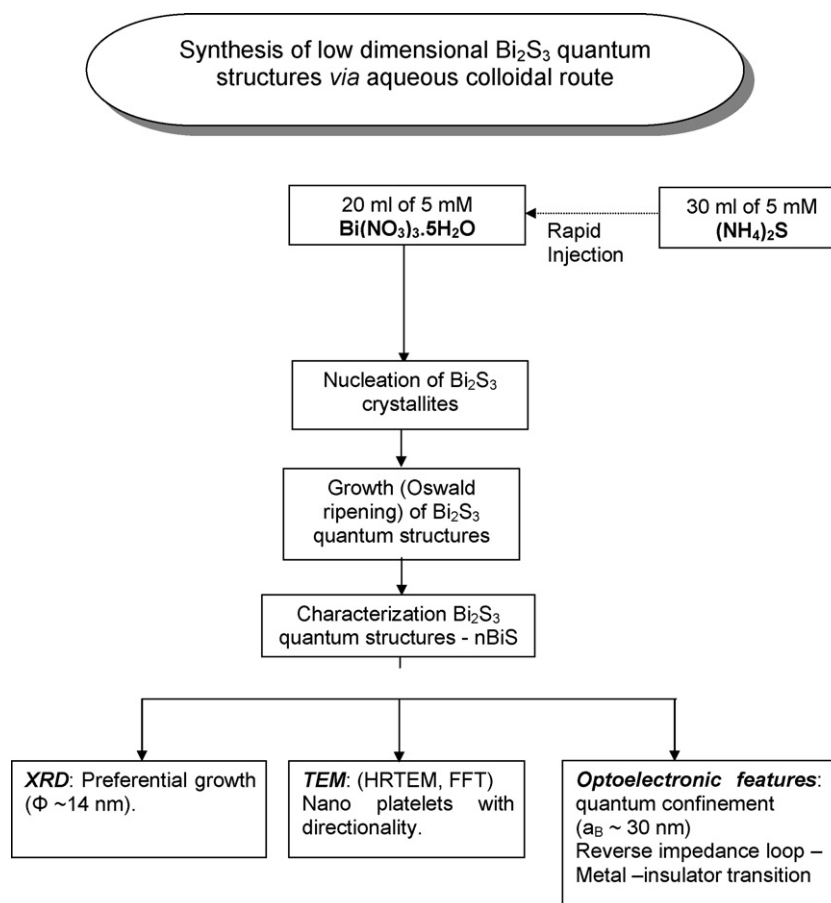


Fig. 1. Flow chart illustrating the synthesis of low dimensional Bi_2S_3 quantum structures via aqueous colloidal route.

tions. Powder X-ray diffraction measurements were done using a PANalytical X-Pert Pro X-ray diffractometer system (using $\text{Cu K}\alpha = 1.5418 \text{ \AA}$ line). TEM and HRTEM images of the nano-particles were obtained using Tecnai-20 G2 instrument of FEI Company operating at 200 kV by placing the colloid on perforated carbon coated Cu sample grid. FFT of the HRTEM image was obtained using a public domain image processing software. Concerning fundamental absorption-edge measurements of nBiS, a Varian Cary-500 UV-vis spectrophotometer was used. Impedance data on these nBiS samples in colloidal form held between smooth aluminum foils as electrodes in a quartz cell were acquired using a Solartron frequency response analyzer (FRA). The impedance measurements were repeated in a time interval of 600 s (for 6 cycles) and the acquired impedance data were fitted using the Z-View software. Also it has been confirmed that the background medium due to ammonium nitrate solution does not contribute to any specific impedance characteristics in the frequency region studied (0.01–10 MHz) to merit any attention while discussing the results of the impedance measurements.

3. Results and discussion

3.1. Directional growth of nBiS

The X-ray diffraction pattern of the as-prepared sample given in Fig. 2 indicates the formation of bismuth sulfide phase. It can be seen that the intensity of the XRD line corresponding to (2 1 1) direction is very prominent suggesting a uni-directional growth of these crystallites. Furthermore, crystallite size estimate on this sample yields using Debye–Scherrer formula a value of

$\sim 14 \text{ nm}$. The bright field transmission electron microscope image given in Fig. 3 shows nearly mono-dispersed particles having two-dimensional disc-like platelet morphology. The particle size distribution obtained from TEM images (Fig. 3a) gives a mean particle size of 11.5 nm with a standard deviation of 1.75 nm, which is nearly the same as the value calculated from XRD peak broadening data. Furthermore, intensity contrast histogram of the image (Fig. 3b) shows two Gaussian like distributions in the image contrast. The narrow peak with lighter contrast is the background intensity

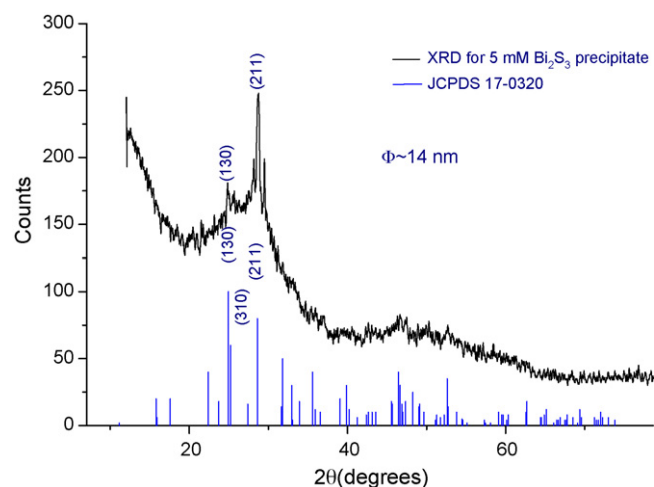


Fig. 2. XRD pattern of bismuth sulfide nanocrystals. Preferential growth along (2 1 1) lattice direction is prominent.

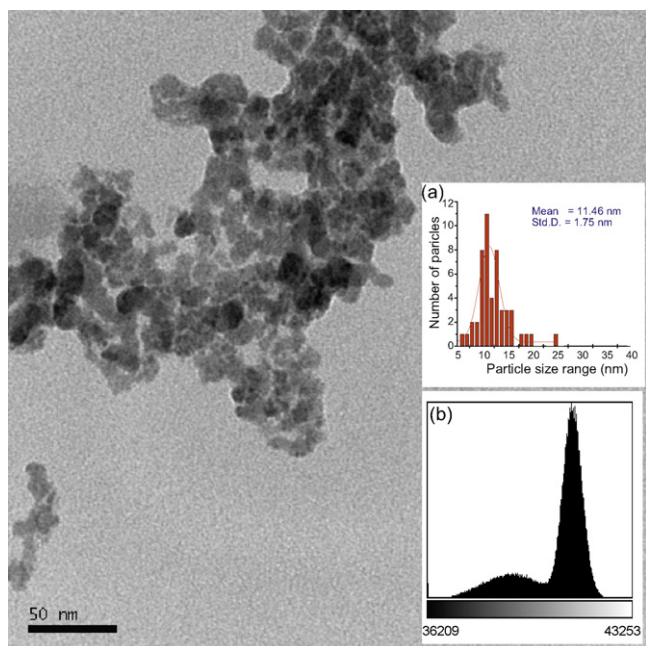


Fig. 3. A representative bright field transmission electron micrograph showing bismuth sulfide quantum structures (nBiS). Inset (a) Histogram of particle size distribution. Inset (b) Histogram of gray levels in the image.

representing the copper grid. The second one on the more darker contrast side is caused by the reduction in electron beam intensity due to nBiS nano-particles. This observation corroborates nearly mono-dispersed nature of the nano-particles distribution having a unique 2D (two-dimensional) morphology of the as-prepared sample. This type of high aspect ratio morphology of bismuth sulfide may arise due to varied thermodynamic stability of different crystallographic planes. The growth of nanocrystals in the solution after nucleation will be such that total surface energy of the nanocrystal is minimized. Furthermore, both HRTEM image and its FFT pattern (Fig. 4a and b) clearly indicate a uni-directional growth of crystallites along (211) lattice vector. It should be noted that there are similar reports with preferential growth on Bi_2S_3 nano-wires, sheets, etc. [7,10,11]. This kind of strategy acquires technological importance for this direct bandgap system having a low bandgap of ~ 1.3 eV with potential for applications in thermoelectric generator,

photovoltaics and X-ray computed tomography. Notwithstanding these design-specific synthesis-strategies, we consider that results of this impedance study on nBiS synthesized using a simple aqueous precipitation-colloidal method appear to be fortuitous as would be discussed subsequently.

The particle size as determined from TEM images (Fig. 3a) is ~ 11 nm, which nearly coincides with the crystallite size, obtained from XRD analysis. This observation may indicate that the crystallites are suspended in the colloid without any appreciable agglomeration. Also it has been found that the nBiS sample without any surface stabilization shows relatively high stability (~ 1 month) without any agglomeration. In view of the large exciton Bohr radius $a_B \sim 30$ nm [13] reported for this system, the investigated nBiS sample can be expected to be in the strong quantum confinement regime as corroborated from the large blue-shift in the bandgap energy ($\Delta E_g \sim 0.7$ eV) from the Tauc plot. Also this blue-shift in the absorption edge coincides with the value found in the literature [14]. Moreover, the ambiguity in fixing the hole and electron effective masses for bismuth sulfide nanocrystals [14,15] can be traced to multifarious morphologies such as 2D and 1D structure formation and highly anisotropic nature of bismuth sulfide semiconductor system.

3.2. Impedance plots and phase element of nBiS

Time resolved impedance plots of the nBiS sample both under Nyquist type and Bode type plots are given in Figs. 5–8 and the variation of fitted parameters are shown in Figs. 9–11 for important frequency regions. The Nyquist type impedance plot comprising the real part of the impedance in the abscissa and the imaginary part in the ordinate also referred as complex plane impedance plot (CPIP). This CPIP for the nBiS sample investigated traces a semi-circular pattern with some additional features as depicted in Fig. 5. A simple semi-circular impedance pattern can be visualized under a parallel resistor–capacitor combination as shown in the equivalent circuit (Fig. 5, inset). In order to describe the results of the major portion of the impedance measurements we need to consider two types of resistance and one kind of capacitance stemming from resistance of the liquid medium constituting the electrolyte part labeled as solution resistance R_s and the other type of resistance referred as charge transfer resistance R_{ct} whilst the capacitive impedance C_{ct} appears to occur in parallel to the charge transfer resistance. It should be noted that in the electrode–electrolyte interface comprising aluminum foil electrode and the nBiS crystallites in the medium

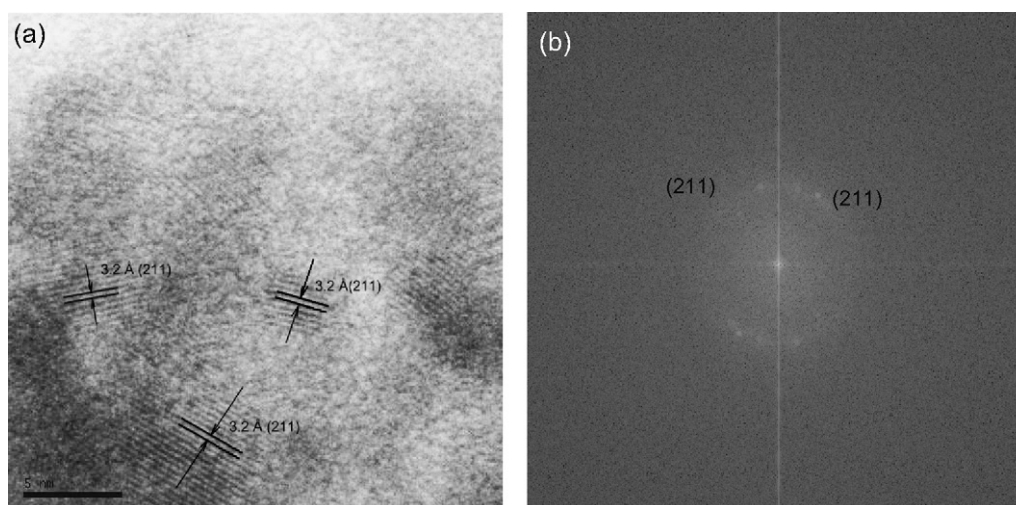


Fig. 4. (a) Representative bright field HRTEM image of bismuth sulfide nanocrystals. (b) Corresponding fast Fourier transform (FFT) image indicating preferential growth along (211) lattice direction.

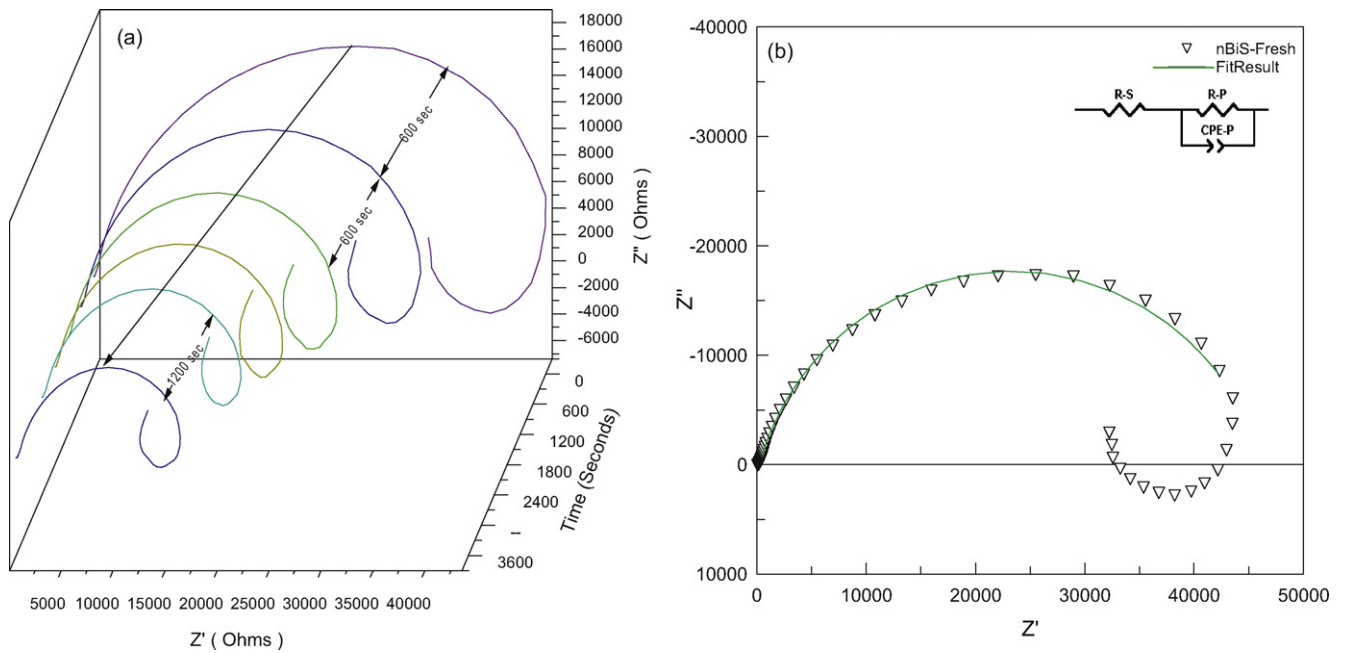


Fig. 5. (a) Time evolution (600-s intervals) of CPIP for the freshly prepared nBiS sample. (b) A representative CPIP for nBiS and its fitted equivalent circuit.

of weak ammonium nitrate electrolyte solution, the charge transfer phenomenon will originate from surface states of the lamellar nBiS crystallites in the vicinity of metal–semiconductor–electrolyte interface. They may get attached or subsequently detached depending on the inter-state population levels, driving mechanism such as adsorption–desorption of SS represented as R_{ads} , C_{ads} or R_{des} , C_{des} , Fermi-level (E_f) mediated equilibration of charge carriers as the case may be (Fig. 12).

Careful comparison of time evolution plots (Figs. 5 and 6) for both fresh and aged nBiS sample makes the following observations and generalizations possible:

- (i) That both fresh and aged sample shows semi-circular profile with nearly similar additional features in the low frequency end. This indicates the presence of a Voigt element and an additional series resistance in all cases, apart from the emerging apparent inductive loop leading to shift towards negative side.
- (ii) For both fresh and aged nBiS samples, as the scan cycle progresses we can observe the center of semi-circles shift towards high frequency side associated with shrinkage both in semi-circle diameter and imaginary part of impedance in the y-axis.
- (iii) The on-set of apparent inductive loop in the low frequency end of the CPIP

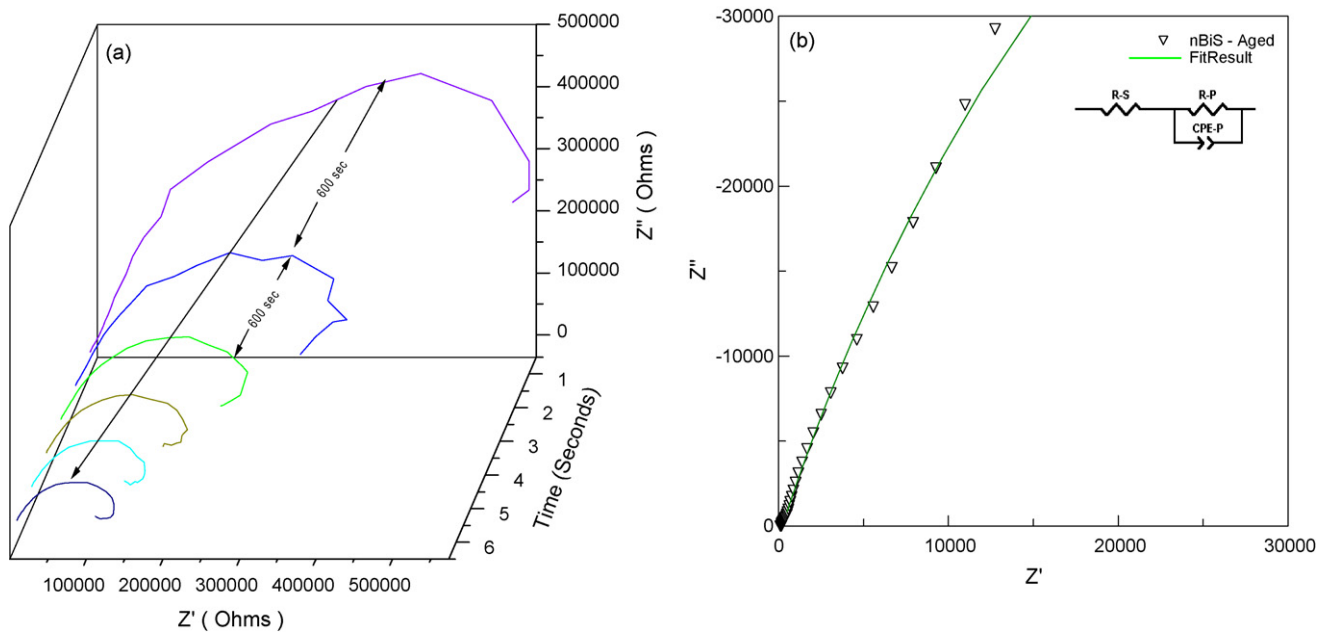


Fig. 6. (a) Time evolution (600-s intervals) of CPIP for the aged nBiS sample. (b) A representative expanded view of CPIP (first run) for the nBiS-aged in the mid-frequency region and its fitted equivalent circuit.

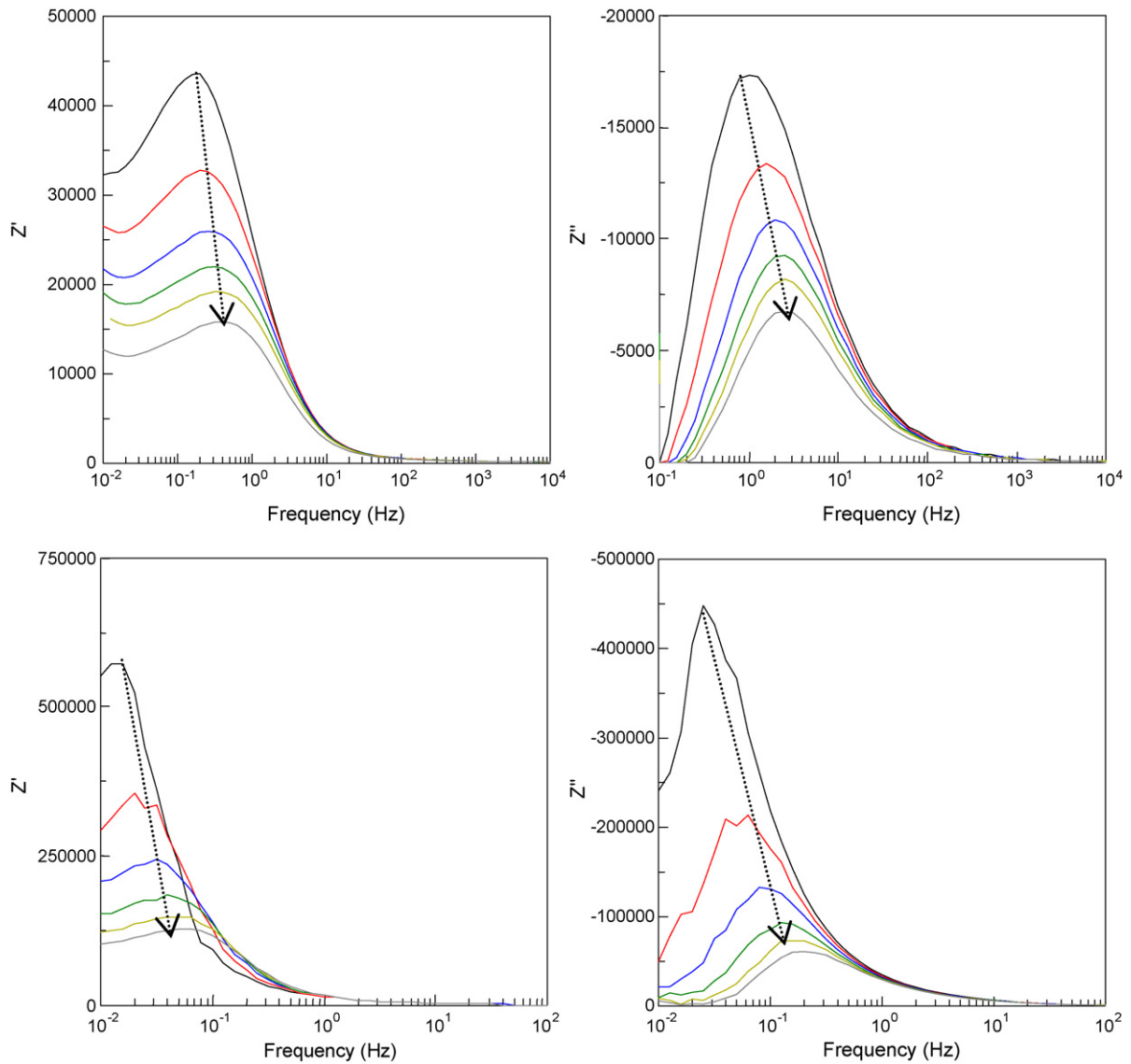


Fig. 7. Bode plots for Z' and Z'' of the fresh and aged nBiS sample. Top row: Fresh nBiS sample. Bottom row: Aged nBiS sample. Arrow indicates the increasing time.

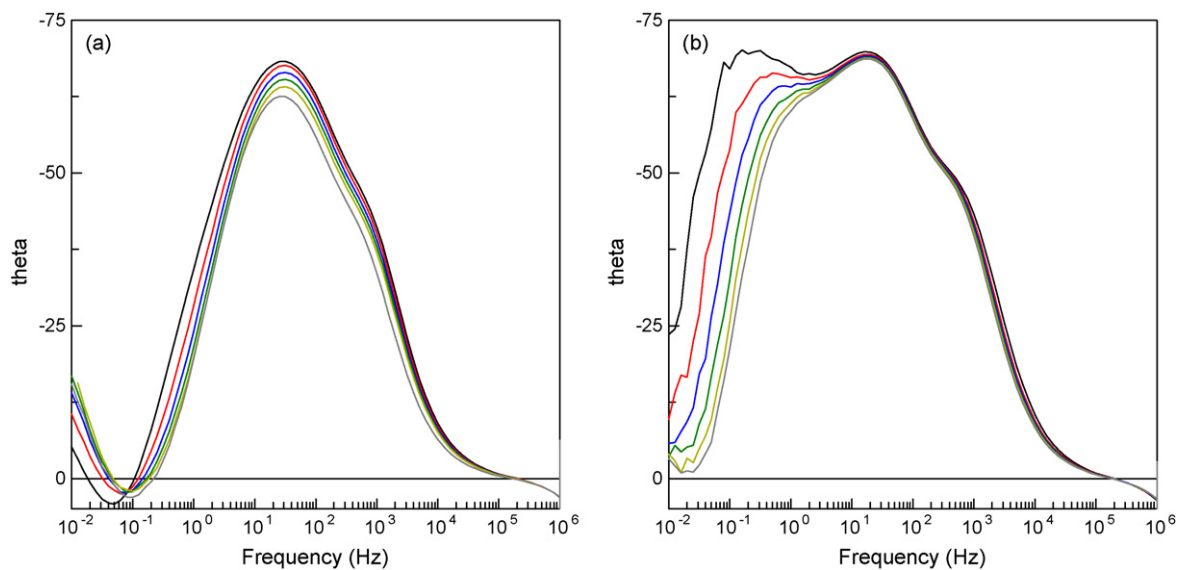


Fig. 8. Time evolution Bode plots for phase angle versus frequency (a) fresh and (b) aged nBiS sample.

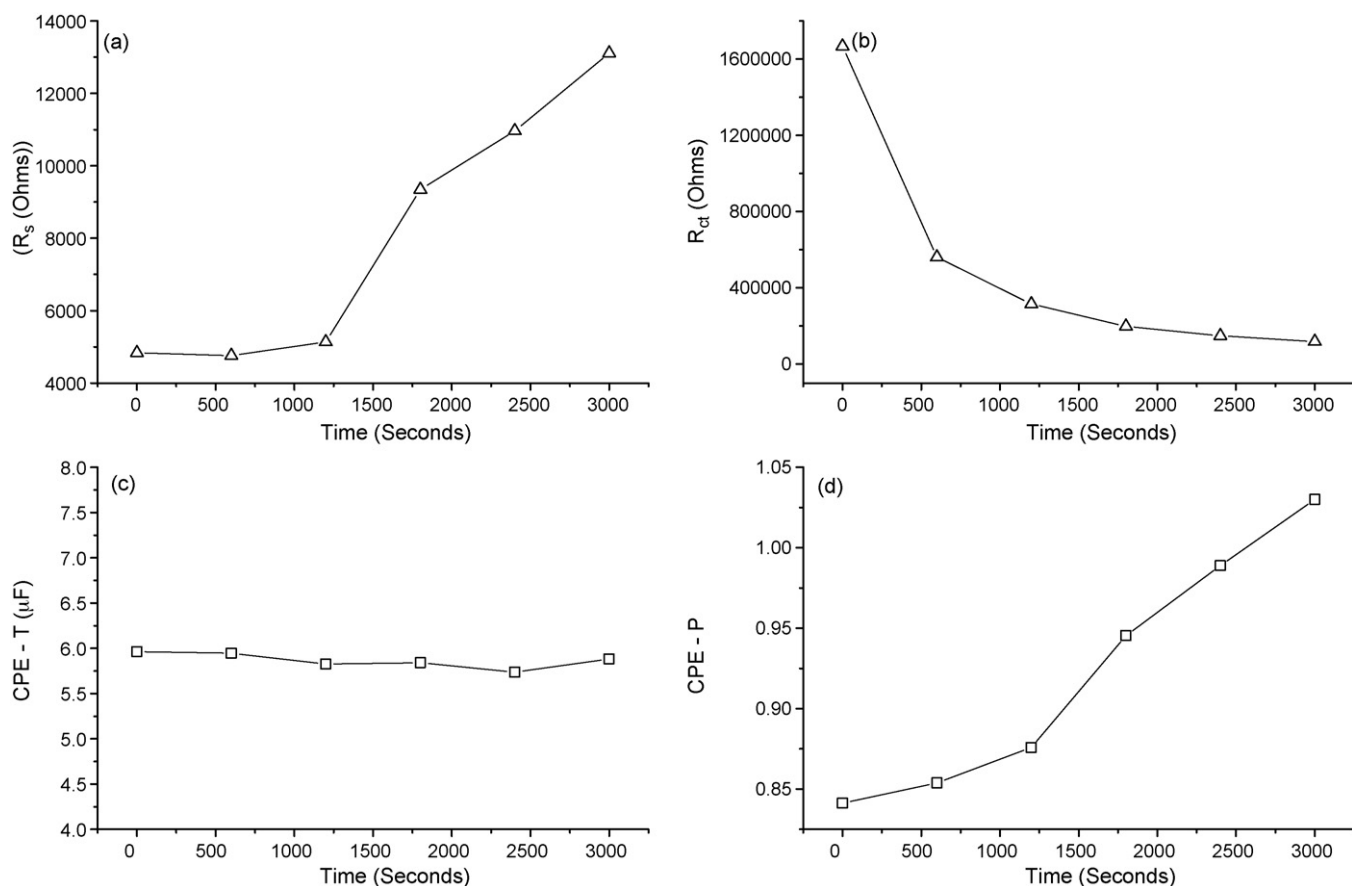


Fig. 9. Time variation plots for different fitted impedance parameters in the low frequency region for nBiS-aged sample. (a) R_s , (b) R_{ct} , (c) CPE-T and (d) CPE-P.

- (iv) In the Bode plot representing frequency dependent variation of real (Z') and imaginary parts (Z'') of impedance profiles (Fig. 7) for both and fresh samples the shift in the impedance maximum towards high frequency in the time evolution plot is very prominent for Z'' consistent with the results of CPIP.
- (v) Furthermore, in the phase angle shift (θ) versus frequency plot, the single band observed for the fresh sample disperses into the multiple bands for the aged sample and further in the low frequency region (~ 0.10 – 0.01 Hz) it dips to negative side (Fig. 8).
- (vi) As the scan cycle increases there is considerable enhancement in capacitance value indicating charge build-up especially in the low frequency end (around 0.05 Hz with the variation being about 30%) corresponding to that of negative impedance region (Table 1)

3.3. Reverse-loop impedance profile vis-à-vis relaxation of surface states

In using impedance spectroscopy to investigate a physico-chemical system, say nano-materials exact description of various circuit elements realized may be more complex than the fitted components. Notwithstanding this, fitting of impedance data and thereby deducing equivalent impedance circuit(s) may be a useful tool to have some reasonable insights on different possible processes associated with nano-material characteristics. The distinguishing feature of this investigation is the occurrence semi-circular profile in the negative y-axis in the low frequency region (~ 0.01 – 0.1 Hz).

Under a CPIP, a semi-circular impedance profile indicates the presence of a Voigt element with the effective impedance being

$$Z_{\text{eff}} = \frac{R_{\text{ads}}}{1 + \omega^2 R_{\text{ads}}^2 C_{\text{ads}}^2} - j \frac{\omega R_{\text{ads}}^2 C_{\text{ads}}}{1 + \omega^2 R_{\text{ads}}^2 C_{\text{ads}}^2} \quad (1)$$

The occurrence of a Voigt element in the present situation can be attributed to numerous surface states which may be present this nano-system and their relaxation characteristics. The impedance measurement condition can be better described by a set two of aluminum foils between which the nBiS semiconductors crystallites enclosed might constitute a parallel plate capacitor set-up (Fig. 12a). In view of large distance (1 cm) between these two foils, the geometrical capacitance expected would be of order of 40 pF (Fig. 12c) and the corresponding semi-circle feature in the CPIP would be in the very high frequency region (~ 1 – 10 MHz). The semi-circular pattern observed in the mid-frequency region (~ 1 – 100 Hz) indicating a high capacitance value of about 5 μF showing pronounced increase in capacitance ($\sim 30\%$) over cycles of measurements. Another important observation that should be mentioned is as the impedance scan cycle proceeds, there is a significant build-up in capacitance (C) accompanied by simultaneous decrease in resistance (R_{ct}) whilst the serial resistance R_s accompanying the Voigt element does not show much change (Figs. 10 and 11). It is important to note that variation in parameter values for the Voigt element is more pronounced for the fresh sample. Furthermore, the Bode type plot representing frequency versus real (Z') and imaginary (Z'') parts of impedance shows that there is significant shift in the peak position corresponding to Z'' shifts towards higher frequency as the scan period increases (Fig. 7). More significantly, the dispersion of the phase angle versus frequency plot into vari-

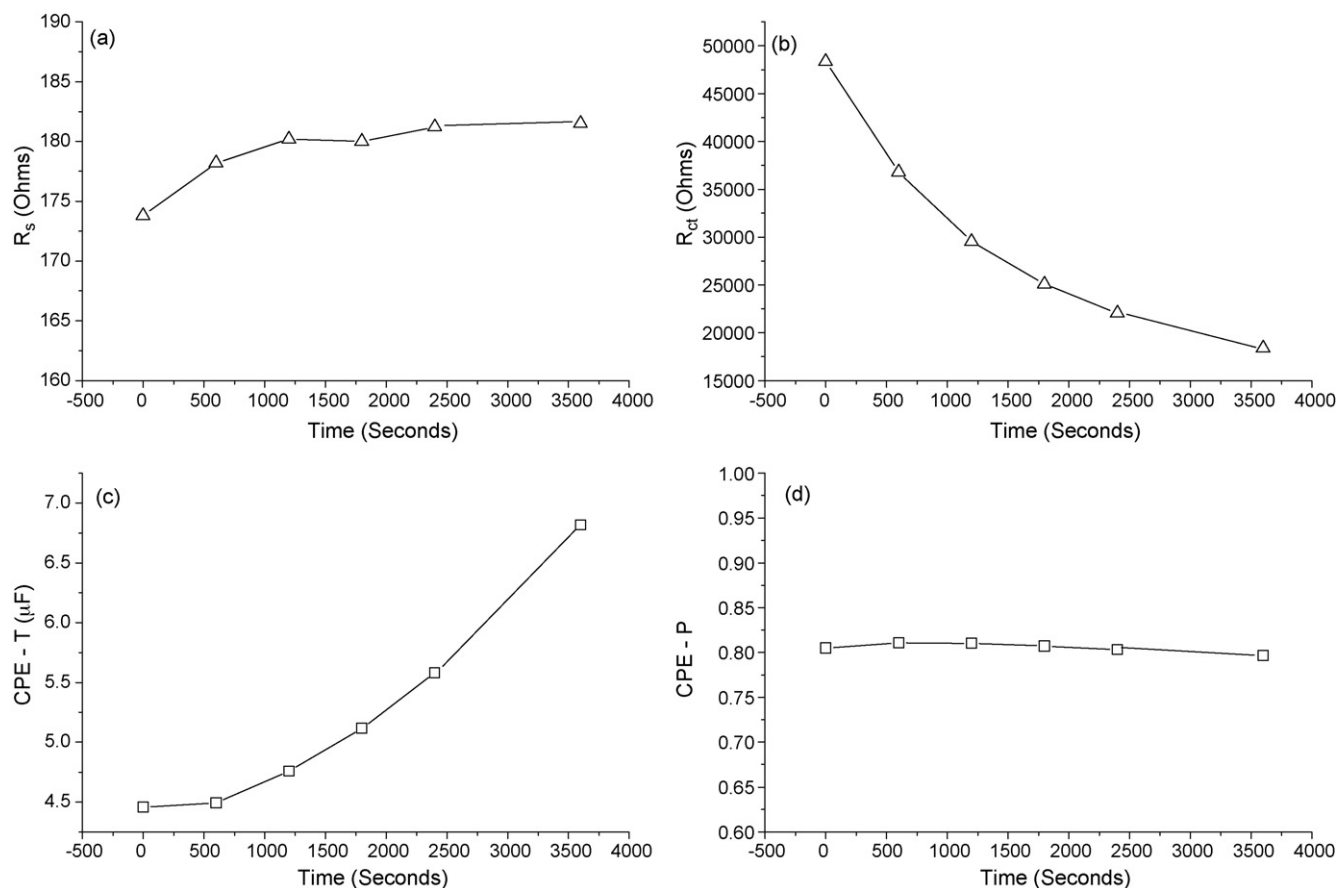


Fig. 10. Variation of fitted impedance parameters in the mid-frequency region for nBiS-fresh sample. (a) \$R_s\$, (b) \$R_{ct}\$, (c) CPE-T and (d) CPE-P.

ous peaks/bands (Fig. 8) only suggesting a temporal charge build-up and multiplicity of processes with different relaxation kinetics.

This prominent semi-circular feature can be attributed to an intense charge accumulation process something like adsorption of surface states in the vicinity of the aluminum electrode foils leading to a resistor–capacitor in parallel combination. Such an intense charge build-up accompanied by considerable decrease in resistivity only points to temporal flow or relaxation of charges. This phenomenon should stem from the relaxation of surface states adsorbed to aluminum electrode foils (Fig. 12c). In all fairness this seems to be more probable. Because in this low bandgap quantum-structured crystallites, creation of numerous charge carriers resulting from surface states, get attracted towards electrode foils and subsequent relaxation will be facilitated by the ammonium nitrate electrolyte medium.

The most distinguishing feature of the impedance study on the nBiS quantum structure is the occurrence of a semi-circle like loop in the negative imaginary axis in the low frequency region. Canonically in a complex plane impedance plot a trace in the negative imaginary side suggests an inductive impedance. There are several

reports on the occurrence of inductive loop in various systems such as ordered metal nanocrystal mono-layer systems [16], platinum anode in a membrane fuel-cell due to carbon monoxide poisoning [17]. But this possibility looks not possible in the present system because fitting the impedance data under an inductive loop asks for a too high value of inductance (~3000 H at this low frequency region) which is not at all possible in a circuit involving a very low current.

Alternatively more plausible mechanism to explain this reverse-loop phenomenon in the negative imaginary axis would be through reversing the signs of resistor–capacitor elements in parallel combination called as negative differential resistor and capacitor [18]. This may arise due to desorption or flow of charges in the reverse direction thereby accounting the negative resistor plus capacitor combination.

Fitting of the negative loop observed in the low frequency region under a negative RC set-up with the effective impedance:

$$Z_{\text{eff}} = \frac{-R_{\text{des}}}{1 + \omega^2 R_{\text{des}}^2 C_{\text{des}}^2} + \frac{\omega R_{\text{des}}^2 C_{\text{des}}}{1 + \omega^2 R_{\text{des}}^2 C_{\text{des}}^2} \quad (2)$$

Table 1

Relative percentage change between fitted impedance parameters of fresh and aged nBiS sample for the first and the fifth impedance scans.

Frequency	ΔR_{ct} (%)		$\Delta \text{CPE-T}$ (%)		$\Delta \text{CPE-P}$ (%)	
	Fresh	Aged	Fresh	Aged	Fresh	Aged
Low F (~0.1–1 Hz)	–45	–91	+38	–4	–2	+18
Mid F (~1–200 Hz)	–54	–23	+25	+11	~0	~0
High F (~200 kHz to 200 Hz)	–20	+3	+20	+10	~0	~0
Very high F (~10 MHz to 200 kHz)	~0	~0	~0	~0	~0	~0

For aged sample CPE-P changes appreciably indicating smoothening of electrode surface due to adsorption of nBiS crystallites.

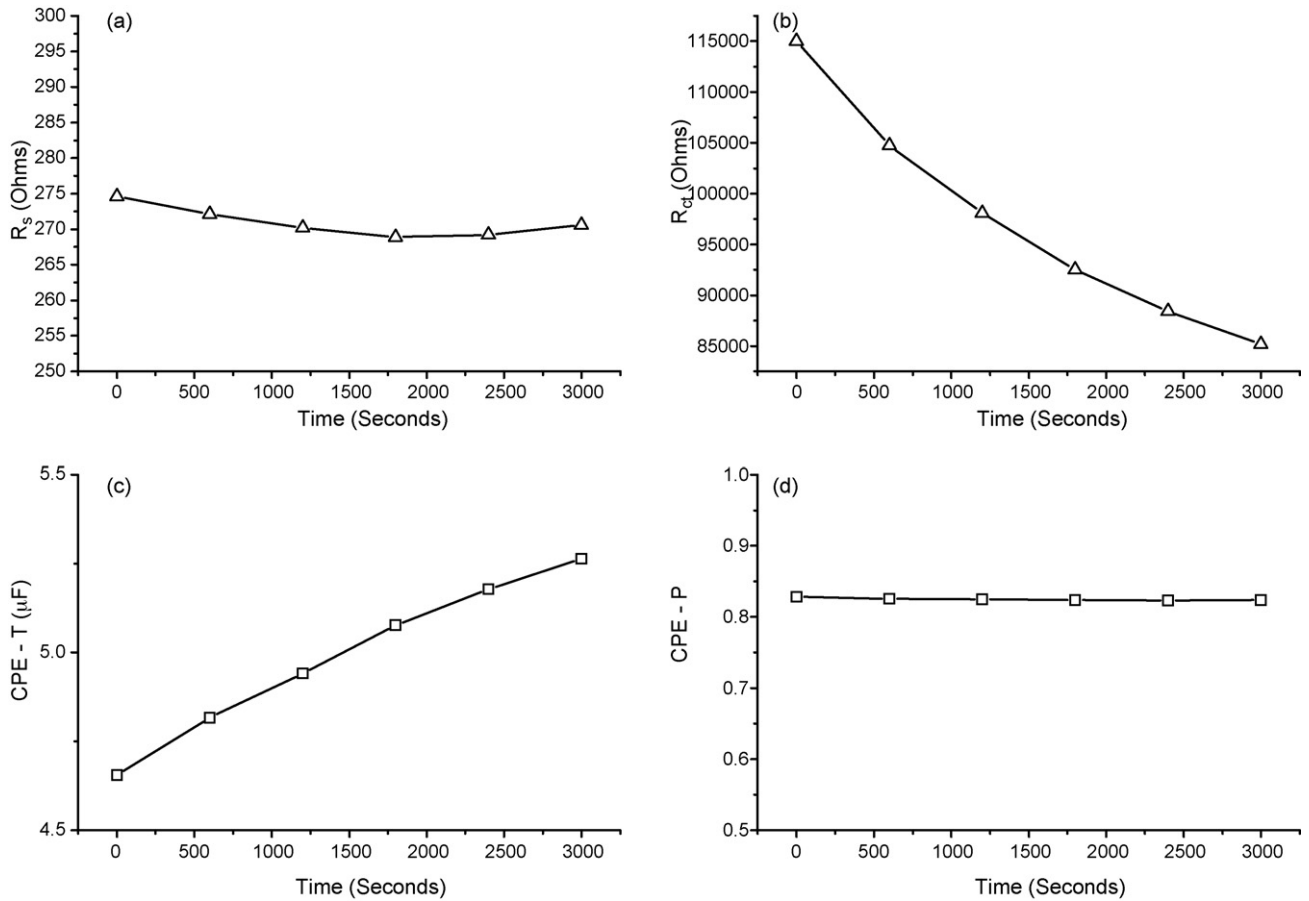


Fig. 11. Variation of fitted impedance parameters in the mid-frequency region for nBiS-aged sample. (a) R_s , (b) R_{ct} , (c) CPE-T and (d) CPE-P.

is remarkably successful (Fig. 13 and Table 2). It should be mentioned that for the aged nBiS sample, the fitting of impedance data in the reverse-loop region seems to be not as effective as for the fresh sample. Notwithstanding this a reasonable fitting has been attempted in this case and possible parameter values are given in Table 2. From this it can be seen that the magnitudes of negative R and C values are two orders higher than that in the positive

side. This may be rationalized in terms of large amount of charge carriers getting depleted in the reverse direction. Obviously this is reflected in the phase angle plot for the aged samples (Fig. 8) wherein the depletion process acquiring prominence in the low frequency region (0.1–0.01 Hz). This adsorption–desorption process entailing in charge build-up due to adsorption (positive capacitance) and negative capacitance due to desorption can be pictorially

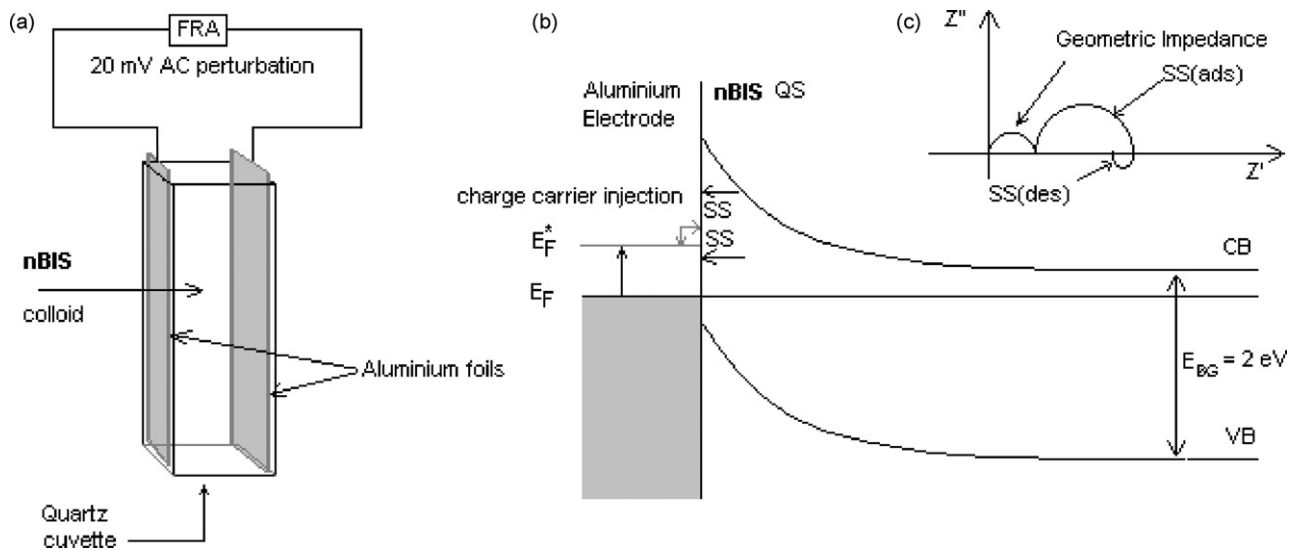


Fig. 12. (a) Experimental setup and (b) energy level diagram of adsorbed nBiS quantum structures. (c) Illustrative CPIP of the sample configuration. FRA, frequency response analyzer; E_F , E_F^* , equilibrium and perturbed Fermi energy levels; SS, surface states adsorbed; QS, quantum structure.

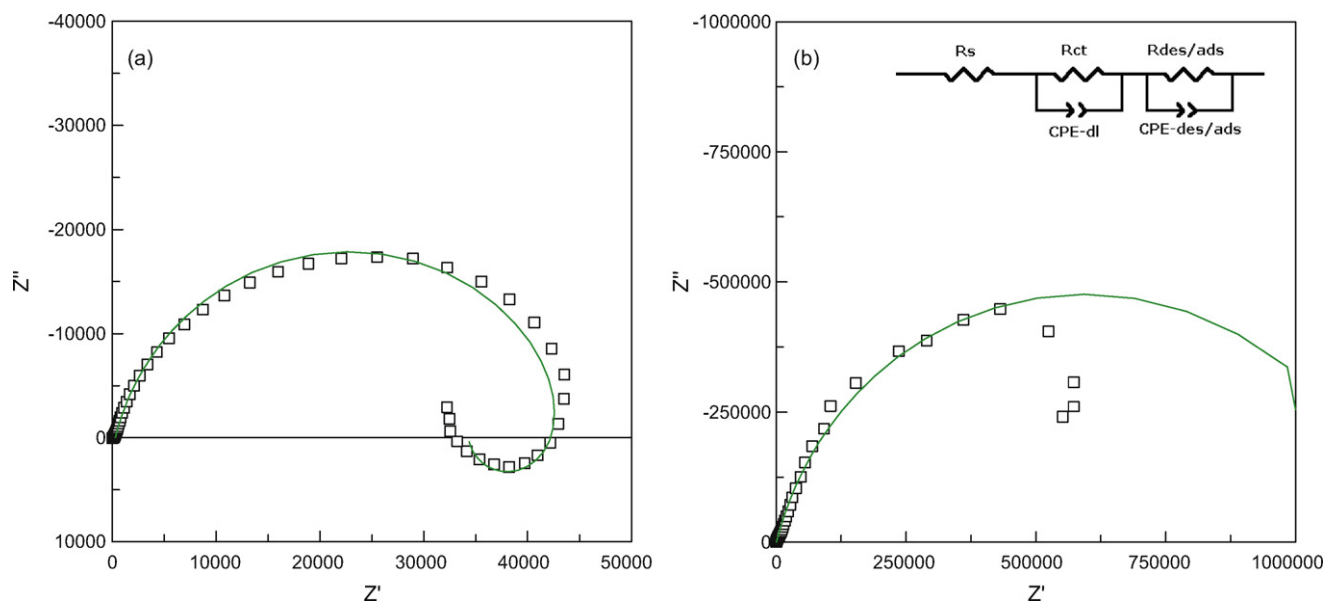


Fig. 13. Fitting of impedance pattern using negative capacitance–resistance model. (a) fresh nBiS and (b) aged nBiS. Inset shows the fitting circuit used.

Table 2

Fitted impedance parameters for reverse loop in the fourth quadrant (using negative R and C parallel combination).

Time (s)	Fresh nBiS $-R$ (Ω)	$-C$ (μF)	Aged nBiS $-R$ (Ω)	$-C$ (μF)
0	13485	313	–	34
600	8875	410	–	24
1200	7321	518	–	41
1800	6677	584	–	74
2400	6388	557	–	112
3000	–	–	–	133
3600	6338	644	–	–

represented as given in the band-energy diagram (Fig. 12). Recently there seems to be some reports on negative capacitance behavior in the low frequency region in several organic light emitting diode systems due to carrier/electron injection in the interface of organic–metal interface [19], organic polymers [20].

4. Concluding remarks

The foregoing results have indicated the pronounced tendency to adsorb–desorb charge carriers which may arise from surface states of nBiS crystallites in the Al–metal–nBiS crystallite (semiconductor) interface in an electrolyte medium. The charge species-carriers may stem from surface states (broken bonds, defects) of the crystallites having some critical size, morphology dependence as evidenced from the absence of this phenomenon for larger crystallites and also unique of this system for it is not observable in a wide-gap nano-ZnS colloids. Curiously, the opt-impedance study [21] on this nBiS sample under UV shining has shown that this negative impedance loop vanishes suggesting a newer scope for fundamental studies on this low bandgap semiconductor quantum structure. Hence, we plan to further expand

the scope of this study through a more quantitative approach on this inorganic semiconducting quantum dots as our future work.

Acknowledgment

Our sincere thanks to Department of Science and Technology, New Delhi for the project grant (100/(IFD)/17/2007-08) and Central Electrochemical Research Institute, Karaikudi–CSIR, New Delhi for the experimental facilities.

References

- [1] S.C. Liufu, L.D. Chen., Q. Yao., C.F. Wang, Appl. Phys. Lett. 90 (2007) 112106.
- [2] R. Suarez, P.K. Nair., P.V. Kamat, Langmuir 14 (1998) 3236.
- [3] O.J. Rabin, M. Perez, J. Grimm, G. Wojtkiewicz, R. Weissleder, Nat. Mater. 5 (2006) 118.
- [4] R.R. Ahire, N.G. Deshpande, Y.G. Gudage, A.A. Sagade, S.D. Chavhan, D.M. Phase, R. Sharma, Sens. Actuators A 140 (2007) 207.
- [5] G. Konstantatos, L. Levina, J. Tang, E.H. Sargent, Nano Lett. 8 (2008) 4002.
- [6] J. Tang, A.P. Alivisatos, Nano Lett. 6 (2006) 2701.
- [7] L. Li, N. Sun, Y. Huang, Y. Qin, N. Zhao, J. Gao, M. Li, H. Zhou, L. Qi, Adv. Funct. Mater. 18 (2008) 1194.
- [8] J. Jiang, S.-H. Yu, W.-T. Yao, H. Ge, G.-Z. Zhang, Chem. Mater. 17 (2005) 6094.
- [9] R. Chen, M.H. So, C.-M. Che, H. Sun, J. Mater. Chem. 15 (2005) 4540.
- [10] X. Cao, L. Li, X. Yi, J. Colloid Interface Sci. 273 (2004) 175.
- [11] B. Michael, B. Sigman Jr., A. Korgel, Chem. Mater. 17 (2005) 1655.
- [12] J. Black, E.M. Conwell, L. Seigle, C.W. Spencer, J. Phys. Chem. Solids 2 (1957) 240.
- [13] B. Pezova, I. Graozdanov, Mater. Chem. Phys. 99 (2006) 39.
- [14] B.F. Variano, D.M. Hwang, C.J. Sandroff, P. Wiltzius, T.W. Jing., N.P. Ong, J. Phys. Chem. 91 (1987) 6455.
- [15] D. Jason Riley, J.P. Wagget, K.G. Upul Wijayantha, J. Mater. Chem. 14 (2004) 704.
- [16] C.P.C. Markovich, J.R. Heath, Phys. Rev. Lett. 80 (1998) 3807.
- [17] N. Wagner, E. Gulzow, J. Power Sources 127 (2004) 341.
- [18] D.R. Franceschetti, J.R. Macdonald, J. Electroanal. Chem. 82 (1977) 271.
- [19] J. Bisquert, G. Garcia-Belmonte, A. Pitarch, Bolink S H.J., Chem. Phys. Lett. 422 (2006) 184.
- [20] H.L. Kwok, Solid-State Electron. 47 (2003) 1089.
- [21] A. Nakkiran, J. Thirumalai, R. Jagannathan, Chem. Phys. Lett. 436 (2007) 155.